Schauer, C. K., Akabori, K., Elliott, C. M., & Anderson, O. P. (1984) *J. Am. Chem. Soc. 106*, 1127–1128.
Siegel, L. M., Murphy, M. J., & Kamin, H. (1973) *J. Biol. Chem. 248*, 251–264.
Siegel, L. M., Rueger, D. C., Barber, M. J., Krueger, R. J., Orme-Johnson, N. R., & Orme-Johnson, W. H. (1982) *J. Biol. Chem. 257*, 6343–6350.
Spiro, T. G., Czernuszewicz, R. S., & Han, S. (1988) in *Biological Applications of Raman Spectroscopy* (Spiro, T. G., Ed.) Vol. 3, pp 523–553, Wiley-Interscience, New York.
Stout, C. D. (1982) *Met. Ions Biol. 4*, Chapter 3.
White, R. H. (1981) *Anal. Biochem. 114*, 349–354.
Yachandra, V. K., Hare, J., Moura, I., & Spiro, T. G. (1983) *J. Am. Chem. Soc. 105*, 6455–6461.

Resonance Raman Studies of *Escherichia coli* Sulfite Reductase Hemoprotein. 3. Bound Ligand Vibrational Modes†

Sanghwa Han,‡ John F. Madden,§ Lewis M. Siegel,*,§ and Thomas G. Spiro‡
Department of Chemistry, Princeton University, Princeton, New Jersey 08540, and Department of Biochemistry, Duke University Medical Center and Veterans Administration Hospital, Durham, North Carolina 27705
Received November 4, 1988; Revised Manuscript Received March 14, 1989

ABSTRACT: The vibrations of the bound diatomic heme ligands CO, CN^-, and NO are investigated by resonance Raman spectroscopy in various redox states of *Escherichia coli* sulfite reductase hemoprotein, and assignments are generated by use of isotopically labeled ligands. For the fully reduced CO complex (ferrous siroheme, reduced Fe_4S_4 cluster) at room temperature, νCO is observed at 1904 cm^{-1}, shifting to 1920 cm^{-1} upon oxidation of the cluster. The corresponding δFeCO modes are identified at 574 and 566 cm^{-1}, respectively, by virtue of the zigzag pattern of their isotopic shifts. In frozen solution, two species are observed for the cluster-oxidized state, with νCO at 1910 and 1936 cm^{-1} and νFeC at 532 and 504 cm^{-1}, respectively; νFeC for the fully reduced species is identified at 526 cm^{-1} in the frozen state. For the ferrous siroheme–NO complex (cluster oxidized), νNO is identified at 1555 cm^{-1} in frozen solution and a low-frequency mode is identified at 558 cm^{-1}; this stretching mode is significantly lower than that observed in Mb–NO. For the ferric siroheme cyanide complexes evidence of two ligand-bonding forms is observed, with modes at 451/390 and 451/352 cm^{-1}; they are distinguished by a reversal of the isotopic shift patterns of the upper and lower modes and could arise from a linear and a bent Fe–C–N unit, respectively. For the ferrous siroheme cyanide complex isotope-sensitive modes observed at 495 and 452 cm^{-1} are assigned to the $FeCN^-$ bending and FeC stretching vibrations, respectively. The possible origin of unusual features of these bound ligand spectra is considered. Distal H-bonding may contribute to these effects, on the basis of the similarity of the reduced CO species to those of an H-bonded form of the CO adduct of horseradish peroxidase.

The hemoprotein subunit (SiR-HP) from *Escherichia coli* sulfite reductase contains a siroheme and an Fe_4S_4 cluster in proximity, as established by X-ray crystallography (McCree et al., 1986). They are magnetically coupled (Janick & Siegel, 1983), and it has been suggested that they are bridged by a common thiolate ligand. In previous papers we have examined the resonance Raman scattering from the siroheme (Han et al., 1989) and the Fe_4S_4 cluster (Madden et al., 1989) in the free enzyme and in several of its stable adducts with exogenous ligands.

On the distal side of the siroheme, opposite the Fe_4S_4 cluster, the X-ray crystal structure does not show significant electron density (McRee et al., 1986). This may be the site where ligands bind to the siroheme, including the substrates SO_3^{2-} and NO_2^-. In the present study we examine RR bands arising from vibrational modes of X–Y diatomic ligands (CO, NO, and CN^-) bound to the siroheme. These include the Fe–X and X–Y stretching modes as well as the Fe–X–Y bending mode. These modes have previously been detected in heme proteins and in protein-free heme complexes, especially in the pioneering studies of Yu and co-workers (Yu, 1986; Kerr & Yu, 1988), via their characteristic isotope shifts. Their enhancement in resonance with the heme electronic transitions is attributed to coupling with the π–π^* excited states. The frequencies and intensities of these modes have been found to provide useful probes of the interactions of the distal ligands with protein side chains around the distal pocket. In particular, distal H-bonding to bound CO produces a downshift in the CO stretching frequency but an upshift in the Fe–C stretching frequency due to the enhanced back-bonding induced by the H-bond interaction (Smulevich et al., 1986; Uno et al., 1987).

In sulfite reductase we find clear evidence for strong perturbation of bound diatomic ligands, probably via distal interactions that may involve H-bonding. An important role for such an interaction is anticipated on the basis of a consideration of the mechanistic requirements of sulfite reduction.

Experimental Procedures

Reagents. $K^{13}CN^-$ (90%), $KC^{15}N$ (99%), $Na^{15}NO_2$ (99%), and ^{13}CO (99%) were from Stohler Isotope Chemicals (Cambridge, MA). $K^{13}C^{15}N$ (99%/99%), $C^{18}O$ (99%), and $^{13}C^{18}O$ (99%/99%) were from Icon Services (Summit, NJ).

† This work was supported by Grant GM 13498 (T.G.S.) and Grant GM 32210 (L.M.S.) from the National Institutes of Health and by Project Grant 7875-01 from the Veterans Administration (L.M.S.). J.F.M. is a fellow of the Medical Scientist Training Progam at Duke University.
‡ Princeton University.
§ Duke University Medical Center and Veterans Administration Hospital.

0006-2960/89/0428-5477$01.50/0

The preparation of ^{18}O-labeled nitrite was a modification of a published method (van Etten et al., 1981). Sodium nitrite, either ^{15}N-labeled or of natural isotopic abundance, was dissolved in 50 μL of $H_2{}^{18}O$ (98%, Cambridge Isotope Laboratories, Woburn, MA) to a concentration of 2 M. While the samples were cooling on ice, 3.3 μL of concentrated HCl was added to each. The mixture was incubated in a sealed vial under inert atmosphere for 22 h at room temperature. The samples were neutralized (pH paper) by the cautious addition of small amounts of 10 N NaOH. The extent of labeling was estimated by RR spectroscopy of the concentrated samples using excitation at 406.7 nm. The feature at 1332 cm^{-1} in natural abundance $NaNO_2$ was observed to shift downward to 1297 cm^{-1} ($Na^{14}N^{18}O_2$), 1311 cm^{-1} ($Na^{15}N^{16}O_2$), or 1272 cm^{-1} ($Na^{15}N^{18}O_2$). Labeling was estimated to be >80% complete in all cases.

Sample Preparation. Sulfite reductase holoenzyme was isolated from *E. coli* B (Siegel & Davis, 1974), and the hemoprotein subunit was separated and further purified as previously described (Han et al., 1989). The oxidized enzyme as isolated (SiR-HP^0) binds exogenous ligands slowly; prior reduction is required to reliably obtain complete conversion to ligand-bound forms (Rueger & Siegel, 1976). Solutions of SiR-HP in 0.1 M potassium phosphate and 100 μM EDTA, pH 7.7 (standard buffer), typically at ~200 μM in heme from on ϵ_{591} = 18 100 M^{-1} cm^{-1} (Janick et al., 1983), were thoroughly deoxygenated by repeated cycles of evacuation and flushing with inert gas. Samples for room temperature RR were prepared in 5-mm-o.d. NMR tubes. The reductant used was the Cr^{II}(EDTA) system that we have previously described (Han et al., 1989). Excess redundant was added, followed by a concentrated stock solution of the ligand (for the CO complexes, the sample container was flushed with CO gas at 1 atm). Reoxidation, if desired, was accomplished by exposure of the sample to air.

Samples for frozen-state RR required higher enzyme concentrations (600–1200 μM) for adequate signal-to-noise ratio. Samples were generated in septum-sealed microvials and were transferred to the sample holder of a low-temperature Raman cell (Czernuszewicz & Johnson, 1983). In the experiments, the fully reduced CO and CN^- adducts were generated from the air-oxidized samples by addition of a small amount of solid sodium dithionite. Further details of sample preparation are presented in the figure legends.

Because Cr(EDTA) can bind anionic ligands (Ogino et al., 1979), care was taken to exclude the possibility that isotope-sensitive bands might arise from the presence of this material in the samples. "No-enzyme" blanks prepared in parallel with the SiR-HP samples were prepared for each of the ligands used here and were examined under the same instrumental conditions; in no case were isotope-sensitive bands detectable. Since the extinction coefficient of Cr(EDTA) in the wavelength range used here is 2–3 orders of magnitude smaller than that of the enzyme, the relative lack of resonance enhancement is as expected. The stable cyanide complex of SiR-HP was also examined after gel filtration to remove Cr^{III}(EDTA) and excess cyanide; the spectrum was identical with that of the untreated sample. Blank samples containing Cr(EDTA) at final concentrations up to 14 mM in the presence of 0.08 mM sodium nitrite gave only broad, poorly resolved bands with no detectable isotope-sensitive components in the spectral regions investigated here.

Raman Spectroscopy. The instrumentation for Raman spectroscopy has been previously detailed (Han et al., 1989). A conventional scanning system is designated in the figure legends "Spex 1402"; a system incorporating an optical multichannel analyzer is designated "Spex 1877".

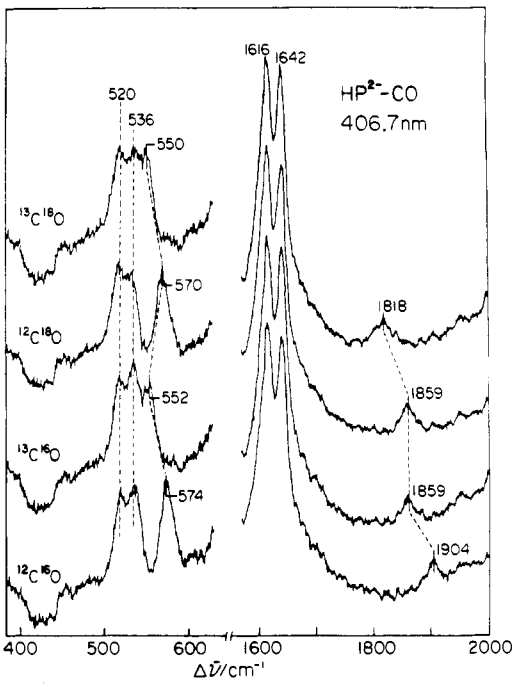

FIGURE 1: RR spectra of SiR-HP^{2-}–CO isotopomers obtained at room temperature with 406.7-nm excitation. To 120 μL of deoxygenated SiR-HP (203 μM) in standard buffer contained in a 5-mm-o.d. NMR tube sealed with a rubber septum was added 10 μL of 14.4 mM Cr^{II}(EDTA) (6-fold molar excess). The tube was flushed with CO gas of the specified isotopic composition, shaken, and allowed to incubate briefly on ice (optical λ_{max} = ~406, 560, and 606 nm). There was no change in the optical spectrum following RR spectroscopy. Instrumental conditions (Spex 1877): power, 150 mW; slit, 150 μm (low frequency), 250 μm (high frequency); integration time, 300 s.

RESULTS

CO Complexes. Figures 1 and 2 show room temperature RR spectra with 406.7-nm excitation of SiR-HP^{2-}–CO and SiR-HP^{1-}–CO with $^{12}C^{16}O$, $^{13}C^{16}O$, $^{12}C^{18}O$, and $^{13}C^{18}O$ isotopomers. The former species is formed by reacting CO with fully reduced homoprotein, SiR-HP^{2-}; it contains the CO adduct of Fe^{II} siroheme and reduced Fe_4S_4 cluster (Janick & Siegel, 1983). It is converted to a SiR-HP^{1-}–CO by exposure to air; the resulting species contains the CO adduct of Fe^{II} siroheme and oxidized Fe_4S_4 cluster. The spectra show isotope-sensitive bands at 1904 cm^{-1} for SiR-HP^{2-}–CO and at 1920 cm^{-1} for SiR-HP^{1-}–CO. These are clearly the CO stretching bands, since they shift down 45 cm^{-1} for ^{13}C or ^{18}O substitution and 86–88 cm^{-1} for $^{13}C^{18}O$ as expected (Yu, 1986). (For SiR-HP^{1-}–CO the 1920-cm^{-1} band is overlapped with a nearby isotope-insensitive feature at ~1945 cm^{-1}, which is an artifact of the diode array detector, but its frequency was reliably determined from a difference spectrum.) The CO stretching bands are weakly but significantly enhanced via the siroheme Soret absorption band, with which the 406.7-nm laser line is near resonance; the intensity is roughly 10% of the intensity of the 1616- and 1642-cm^{-1} siroheme bands, which are among the strongest in the spectrum. This enhancement is qualitatively similar to that seen for the CO adducts of myoglobin and hemoglobin (Tsubaki et al., 1982).

Other isotope-sensitive bands are seen at 574 and 566 cm^{-1} for SiR-HP^{2-}–CO and SiR-HP^{1-}–CO, respectively. These frequencies are in the range of FeCO bending frequencies for several heme proteins (Tsubaki et al., 1982; Yu et al., 1984; Smulevich et al., 1986; Uno et al., 1987), and both bands show the characteristic zigzag isotope pattern of a bending mode:

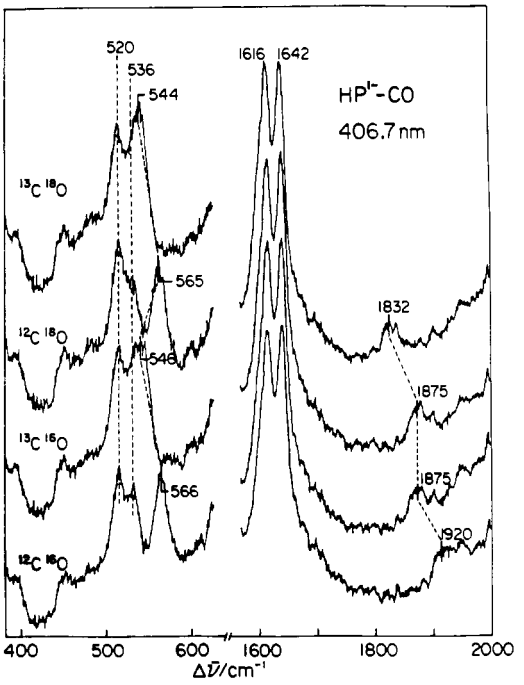

FIGURE 2: RR spectra of SiR-HP^{1-}–CO isotopomers obtained at room temperature with 406.7-nm excitation. Into the tubes containing the samples shown in Figure 1 was injected 80 μL of air. The tube were shaken on ice until no further change in the optical spectrum was observed (optical λ_{max}) = ~402, 558, and 600 nm). There was no change in the optical spectrum following RR spectroscopy. Instrumental conditions (Spex 1877): same as Figure 1.

^{13}C substitution produces a much larger downshift than does ^{18}O substitution. This pattern results from the fact that the C atom moves much more than the O atom when the linear Fe–C–O system bends; a simple vibrational calculation captures this effect (Yu et al., 1984; Li & Spiro, 1988). The FeCO bending mode stands out clearly in these spectra and is as strongly enhanced as the siroheme modes at 520 and 536 cm^{-1}. While these siroheme bands are relatively weak (about one-fifth the intensity of the 1616- and 1642-cm^{-1} bands), the enhancement of the FeCO bending mode is nevertheless impressive. In heme proteins the enhancement of this mode is variable. It is not seen at all in protein-free heme–CO complexes unless there is steric hindrance to the normal perpendicular bonding of the CO ligand (Yu et al., 1983). Its intensity in heme proteins has therefore been connected with the off-axis bonding of CO (Yu et al., 1983), probably via tilting of the entire FeCO unit relative to the heme plane. Off-axis bonding is seen in the crystal structure of CO–myoglobin (Kuriyan et al., 1986) and other heme proteins (Heidner et al., 1976; Baldwin, 1980; Steigmann & Weber, 1979). It has been pointed out elsewhere (Li & Spiro, 1988), however, that the requirement for RR enhancement of the FeCO bend is a lowering of the fourfold heme–CO symmetry, which could be provided by an asymmetric electronic environment as well as by off-axis bonding per se. In the case of SiR-HP, the fourfold symmetry is intrinsically broken by the reduction of two adjacent pyrrole rings of the siroheme macrocycle, and the FeCO bending mode may be intrinsically activated for this reason. Studies of isolated siroheme or isobacteriochlorin models will be needed to evaluate the protein influence on this band. By analogy with heme CO adducts, the FeC stretch is expected in the 480–540-cm^{-1} region (Yu, 1986). Only the siroheme bands at 520 and 536 cm^{-1} are seen in this region in the temperature spectra (see Figures 1 and 2).

In the spectra of frozen samples obtained at 77 K, as shown in Figures 3 and 4, significant differences from the room

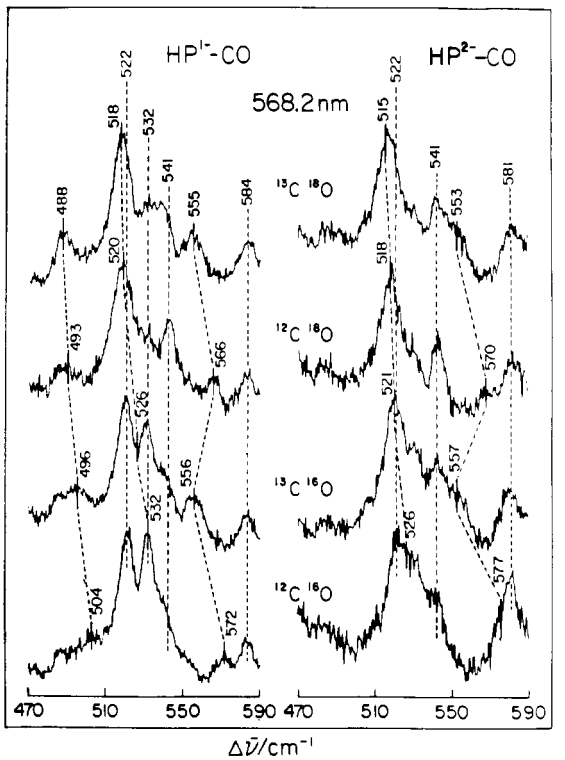

FIGURE 3: RR spectra of SiR-HP^{1-}–CO and SiR-HP^{2-}–CO isotopomers obtained at 77 K with 568.2-nm excitation. To 25 μL of deoxygenated SiR-HP (603 μM) in standard buffer contained in a microvial flushed with CO gas of the specified isotopic composition was added 25 μL of 24.6 mM Cr^{II}(EDTA) (40-fold molar excess). The sample was allowed to incubate on ice for 15 min, opened briefly to air, and then immediately frozen. Optical spectroscopy of a diluted aliquot of the air-oxidized sample showed λ_{max} = 402, 558, and 600 nm. The RR spectra were obtained first on the oxidized sample in the frozen state (77 K); the unused portion was thawed, reduced to the HP^{2-}–CO state by the addition of a small crystal of sodium dithionite, and refrozen. Instrumental conditions (Spex 1402): power, 120 mW; slit, 4 cm^{-1}; scan increment, 0.5 cm^{-1}; acquisition time, 4 s/point.

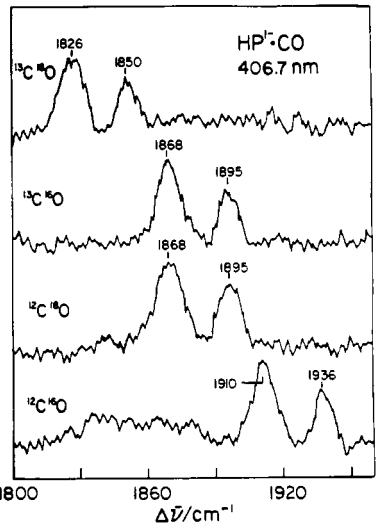

FIGURE 4: RR spectra of SiR-HP^{1-}–CO isotopomers in the CO stretching frequency region obtained at 77 K with 568.2-nm excitation. Preparation as in Figure 3. Instrumental conditions (Spex 1402): power, 120 mW; slit, 10 cm^{-1}; scan increment, 1 cm^{-1}; acquisition time, 10 s/point.

temperature samples are observed. The high-frequency RR spectrum of frozen SiR-HP^{1-}-CO obtained with 406.7-nm excitation (Figure 4) contains two distinct bands, at 1910 and 1936 cm^{-1}, both of which show the proper isotope shifts for

a CO stretching vibration. These frequencies bracket the 1920-cm^{-1} frequency observed in the room temperature spectra (Figure 2). Attempts to examine the CO stretching modes of frozen SiR-HP^{2-} were unsuccessful. In the low-temperature spectra the FeCO bending mode can still be tracked via the zigzag isotope pattern, although its enhancement is now weaker relative to nearby siroheme bands, seen at 584, 541, 532, and 522 cm^{-1}. The additional siroheme bands, relative to the 406.7-mm spectra (Figures 1 and 2), are associated with the altered enhancement factors at 568.2 nm. The low-temperature samples display a frequency upshift of the bending modes, by 3 cm^{-1} for SiR-HP^{2-}–CO to 577 cm^{-1} and by 6 cm^{-1} in SiR-HP^{1-}–CO to 572 cm^{-1}. The FeC stretch is expected to show a monotonic decrease in frequency with increasing mass of the ligand. It can be identified at 526 cm^{-1} in SiR-HP^{2-}–CO, shifting to 515 cm^{-1} in the $^{13}C^{18}O$ isotopomer, and at 532 cm^{-1} in SiR-HP^{1-}–CO shifting to 518 cm^{-1} in the $^{13}C^{18}O$ isotopomer. The siroheme bands at 522 and 532 cm^{-1} overlap the FeC stretching band, and consequently its frequency is difficult to establish in the intermediate isotopomers, $^{13}C^{16}O$ and $^{12}C^{18}O$. The band shifts between $^{12}C^{18}O$ and $^{13}C^{18}O$ spectra are quite clear-cut, however. These spectra were taken with 568.2-nm excitation, in resonance with the siroheme Q band, but similar results are obtainable at 406.7 nm, although the FeC band is less enhanced at this wavelength. We note that for porphyrins the FeC stretch and FeCO bending modes are not seen with Q-band excitation; their enhancement at 568.2 nm for sulfite reductase reflects the stronger Q-band oscillator strength and consequently the greater A term RR enhancement in the case of siroheme. In SiR-HP^{1-}–CO we see an additional, weak band at 504 cm^{-1}, which shifts monotonically with increasing CO mass and is also assignable to FeC stretching. The observation of two FeC stretching bands confirms the presence of two distinct forms of bound CO.

A point of considerable interest is the remarkable photostability of both SiR-HP^{2-}–CO and SiR-HP^{1-}–CO. We saw no evidence in the RR spectra for photodissociation even with laser powers of 400 mW; even stationary samples showed no photoeffects if kept cool. These observations are consistent with the reported failure to see an absorption transient upon photoexcitation of the CO adduct (Murphy et al., 1974). Since heme–CO adducts are ordinarily highly photolabile, we attribute the photostability to rapid recombination.

NO Complexes. Figure 5 shows spectra of the NO adduct, SiR-HP^{1-}–NO, obtained by reaction of SiR-HP^{2-} with NO_2^- until excess reductant is exhausted; the species contains oxidized Fe_4S_4 cluster and the NO complex of Fe^{II} siroheme (Janick & Siegel, 1983; Janick et al., 1983). These spectra were obtained on frozen solutions and reveal two isotope-sensitive bands. The one at 558 cm^{-1} shows a clear zigzag pattern, just like the 554-cm^{-1} band of the NO adduct of Fe^{II} myoglobin and hemoglobin (Tsubaki & Yu, 1982). This band has been assigned to the FeNO bending mode by Benko and Yu (1983), although a mixture of stretch and bend is a better description (Li & Spiro, 1988) since the FeNO equilibrium configuration is bent. The band at 1555 cm^{-1} is clearly assignable to NO stretching, shifting down 30 cm^{-1} for $^{15}N^{16}O$, 36 cm^{-1} for $^{14}N^{18}O$, and 54 cm^{-1} for $^{15}N^{18}O$. This frequency is significantly lower than that seen for the myoglobin adduct, 1624 cm^{-1} (Tsubaki & Yu, 1982).

Although SiR-HP^{1-}–NO can be oxidized to a Fe^{III} siroheme adduct by addition of ferricyanide, we were unable to obtain its RR spectrum due to facile photoreduction at room temperature and to an uncharacterized photodecomposition reaction at 77 K. Similar instability is seen for other Fe^{III}–NO heme adducts (Benko & Yu, 1983). Only for horseradish peroxidase and myoglobin has the Fe^{III}–NO adduct been characterized by RR spectroscopy (Benko & Yu, 1983). This species is isoelectronic with the Fe^{II}–CO adduct, and the vibrational pattern is analogous, although the FeN stretching frequency is considerably higher than the FeC stretching frequency and the NO stretching frequency (Maxwell & Caughey, 1976) is considerably lower than the CO stretching frequency, due to enhanced back-bonding in the Fe^{III}–NO complex. Similar effects are seen in isoelectronic Mn^{II}–NO adducts (Parthasarathi & Spiro, 1987).

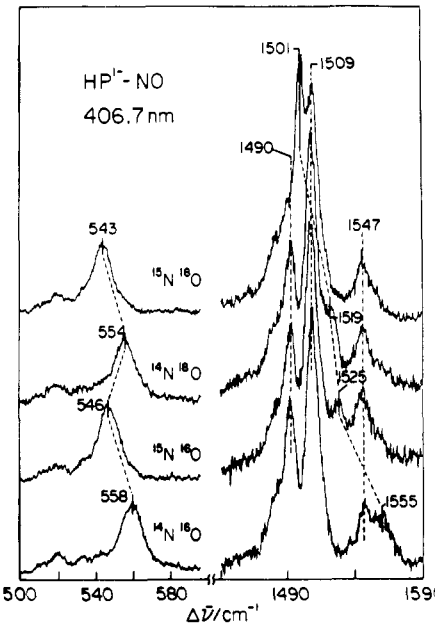

FIGURE 5: RR spectra of SiR-HP^{1-}–NO isotopomers obtained at 77 K with 406.7-nm excitation. To 15 μL of deoxygenated SiR-HP (1.12 mM) in standard buffer was added 5 μL of 25.9 mM Cr^{II}(EDTA) (7.7-fold molar excess), followed by 1 μL of 0.2 M $NaNO_2$ (12-fold molar excess, final $[NO_2^-]$ = 10 mM) of the specified isotopic composition (see Experimental Procedures) in standard buffer. Sample preparation was carried out within the anaerobic glovebox. Optical spectroscopy on aliquots of the samples using a thin-layer optical cell constructed by using microscope cover slips gave λ_{max} = 398 and 596 nm. Instrumental conditions (Spex 1402): power, 120 mW; slit, 7 cm^{-1}; scan increment, 1 cm^{-1}; acquisition time, 4 s/point (low frequency), 2 s/point (high frequency).

Figure 6 shows that the 558-cm^{-1} Fe–NO band can also be seen at room temperature, although it is somewhat weakened relative to the nearby siroheme bands and its frequency is lowered by 10 cm^{-1}. This shift is in the same direction but larger than those seen for the CO adducts. Similar enhancement of this band is seen with 568.2-nm excitation. A point of some interest is that the 558-cm^{-1} band can also be seen with 457.9-nm excitation, albeit weakly. At this wavelength siroheme modes are suppressed but Fe_4S_4 cluster bands are optionally enhanced (Madden et al., 1989).

CN^- Adducts. Figure 7 shows RR spectra of frozen samples of SiR-HP^{2-}–CN^- with 413.1- and 568.2-nm excitation. Both spectra show a 495-cm^{-1} band with a zigzag isotope pattern, which is assignable to the $FeCN^-$ bending mode of a linear Fe–CN^- complex. The FeC stretch can be identified in the 568.2-nm-excited spectrum at 452 cm^{-1} by its monotonic shift with increasing cyanide mass. Interestingly, this band is not observed with 413.1-nm excitation. The situation is similar to that encountered for the CO adducts, in which the FeC stretches are more clearly discernible with Q-band than with Soret-band excitation. There have been no previous reports

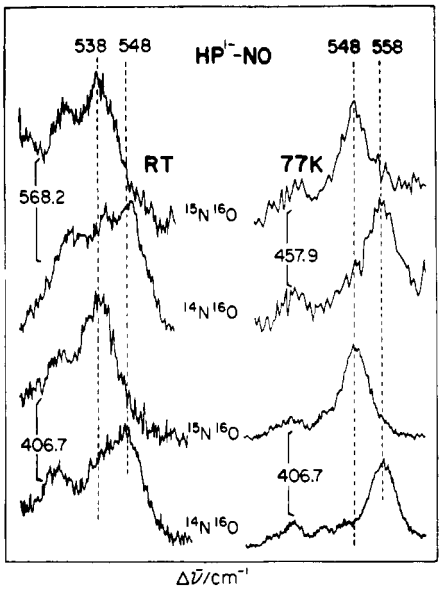

FIGURE 6: RR spectra of SiR-HP^{1-}–NO obtained at room temperature and 77 K with Soret (406.7 nm) and Q-band (568.2 nm) excitation. Room temperature: To 100 μL of deoxygenated SiR-HP (225 μM) in standard buffer contained in a 5-mm-o.d. NMR tube was added 25 μL of 10 mM Cr^{II}(EDTA) (11-fold molar excess), followed by 10 μL of 0.1 M $NaNO_2$ (44-fold molar excess, final [NO_2^-] = 7.5 mM) of the specified isotopic composition (see Experimental Procedures) in standard buffer (optical λ_{max} = 596 nm). 77 K: Same as in Figure 5. Instrumental conditions (Spex 1402): power, 100 mW; slit, 7 cm^{-1}; scan increment, 1 cm^{-1}; acquisition time, 8 s/point.

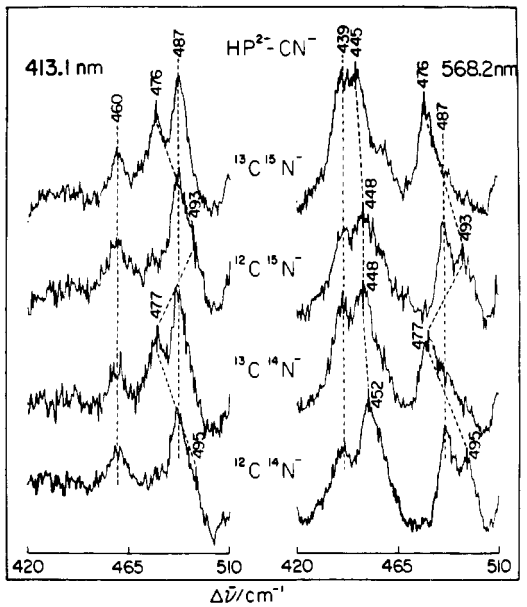

FIGURE 7: RR spectra of SiR-HP^{2-}–CN$^-$ isotopomers in the ligand vibrational frequency region obtained at 77 K with Soret (413.1 nm) and Q-band (568.2 nm) excitation. Samples were prepared as described in the legend to Figure 8. Prior to RR spectroscopy the sample was thawed in the glovebox and a small crystal of sodium dithionite was added to generate the HP^{2-}–CN species. Instrumental conditions (Spex 1402): power, 100 mW; slit, 0.5 cm^{-1}; scan increment, 1 cm^{-1}; acquisition time, 2 s/point (413.1 nm), 6 s/point (568.2 nm).

of heme Fe^{II}–CN$^-$ RR bands with which comparisons might be made.

The FeC stretching and FeCN$^-$ bending RR bands have been recorded, however, for the Fe^{III}–CN$^-$ complex of an insect hemoglobin (Yu et al., 1984; Gersonde et al., 1987). The frequencies 453 and 412 cm^{-1} show monotonic and zigzag isotope dependencies, respectively. The 568.2-nm-excited spectra of SiR-HP^0–CN$^-$ (Figure 8) show similar features.

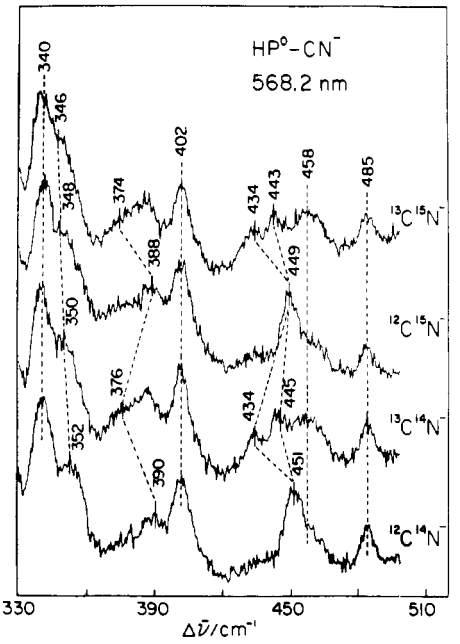

FIGURE 8: RR spectra of SiR-HP^0–CN$^-$ isotopomers obtained at 77 K with 568.2-nm excitation. To 25 μL of deoxygenated SiR-HP (603 μM) in standard buffer was added 8 μL of 25 mM Cr^{II}(EDTA), followed by 2 μL of 0.25 M KCN of the specieid isotopic composition that had been neutralized with HCl. The sample was incubated briefly on ice and then opened to the air before freezing. Optical spectroscopy of a diluted aliquot of the sample gave λ_{max} = 405 and 581 nm. Instrumental conditions (Spex 1402): power, 120 mW; slit, 4 cm^{-1}; scan increment, 0.5 cm^{-1}; acquisition time, 8 s/point.

The 390-cm^{-1} band has a zigzag isotope dependence, while the 451-cm^{-1} band shows a nearly monotonic decrease with increasing mass; the shift to 443 cm^{-1} for $^{13}C^{15}N^-$ is nearly the same as that shown by the insect hemoglobin 453-cm^{-1} band.

In addition, however, there are two other isotope-sensitive features in the SiR-HP^0–CN$^-$ spectrum: a monotonically decreasing band at 352 cm^{-1} and a second band at 451 cm^{-1} with a zigzag isotope dependence. The overlapped 451-cm^{-1} bands are clearly separated in the $^{13}C^{14}N^-$ and $^{13}C^{15}N^-$ spectra. The coexistence of these two pair of bands implies that there are two different forms of bound CN$^-$ in the oxidized hemoprotein, just as there are two forms of bound CO in SiR-HP^{1-}–CO. A more profound structural difference between the two forms of bound CN$^-$ is implied, however, by the reversal of the isotope shift pattern. The form similar to that found in insect hemoglobin has the zigzag mode lower than the monotonic mode, while the reverse is true for the second form.

We tried unsuccessfully to observe the C–N stretching mode in SiR-HP^{2-}–CN$^-$ and SiR-HP^0–CN$^-$. No RR band associated with this mode has been reported for heme–CN$^-$ complexes, although it has been detected via infrared spectroscopy (Yoshikowa et al., 1985). The IR band is found at 2131 and 2029 cm^{-1} in the CN$^-$ adducts of Fe^{III} and Fe^{II} horseradish peroxidase, respectively. The Soret-excited RR spectrum of SiR-HP^0–CN$^-$ could not be obtained because of photoinstability. When excited with violet laser lines, the SiR-HP^0–CN$^-$ samples photodecomposed to uncharacterized species; the nature of this photoeffect is not known.

Discussion

Vibrational Characteristics of Bound XY Ligands. The diatomic ligands, XY, included in this study, CO, NO, and CN$^-$, share several characteristics. They contain multiple bonds between first-row atoms, which are much lighter than the Fe atom to which they are bound. Consequently, the XY

Table I: Raman Frequencies (cm^{-1}) of Ligand Vibrational Modes of SiR-HP

species	model I[a]	mode II[b]	ν(X–Y)[c]	ref
HP^{2-}–CO				
RT	–	574 (22, 4, 24)[d]	1904 (45, 45, 86)	this work
77 K	526 (5, 8, 11)	577 (20, 7, 24)	–	this work
HP^{1-}–CO				
RT	–	566 (20, 1, 22)	1920 (45, 45, 48)	this work
77 K	532 (6, 12, 14)	572 (16, 6, 17)	1910 (42, 42, 84)	this work
	504 (8, 11, 16)	–	1936 (41, 41, 86)	this work
HRP–CO				
low pH	537 (4, 8, –)	587 (20, 0, –)	1904	Smulevich et al. (1986)
high pH	490 (5, 10, –)	–	1932	Smulevich et al. (1986)
Hb–CO (CTT III)	500 (5, 11, 13)	574 (17, 4, 17)	1960 (42, 42, 85)	Yu et al. (1984)
HP^{1-}–NO				
RT	–	548 (10, 5, 13)		this work
77 K	–	558 (12, 4, 15)	1555 (30, 36, 54)	this work
Mb–NO	–	554 (9, 0, –)	1624 (37, –, –)	Tsubaki and Yu (1982) and Benko and Yu (1983)
HP^{2-}–CN^-, 77 K	452 (4, 4, 7)	495 (18, 2, 18)	–	this work
HP^{0}–CN^-, 77 K	451 (6, 2, 8)[e]	390 (14, 2, 16)	–	this work
	352 (2, 4, 6)	451 (17, 2, 17)	–	this work
Hb–CN^- (CTT III)	453 (3, 3, 7)	412 (9, 0, 9)	–	Yu et al. (1984)

[a] Mode that shows monotonic downshifts for XY → *XY → X*Y → *X*Y (*X denotes ^{13}C for CO and CN^- or ^{15}N for NO and *Y denotes ^{18}O for CO and NO or ^{15}N for CN^-) substitutions. [b] Mode that shows a zigzag pattern. [c] Stretching mode of C–O, N–O, or C–N. [d] Numbers in parentheses are the observed isotope shifts for *XY, X*Y, and *X*Y, respectively. [e] This band does not show a purely monotonic downshift.

stretch is at much higher frequency and is nearly decoupled from the FeX stretching or FeXY bending modes. The latter two vibrational modes are in the same frequency range for all three ligands, 300–600 cm^{-1} (Yu, 1986). CO, NO, and CN^- all form low-spin heme complexes, in which back-bonding is important since the π^* orbitals associated with the multiple XY bonds can accept the iron d_π electrons. Back-bonding weakens the XY bond strengthens the FeX bond, with concomitant changes in the stretching frequencies.

When the FeXY unit is linear, the FeXY bending mode is uncoupled from the FeX and XY stretches by symmetry. The bending mode is non totally symmetric, since it destroys the symmetry axis, while the stretching modes are symmetric. The FeXY bend may be higher or lower in frequency than the FeX stretch. In Fe^{II}–CO heme adducts the stretch is lower than the bend (Tsubaki et al., 1982; Yu et al., 1984; Smulevich et al., 1986; Uno et al., 1987), but in the isoelectronic Fe^{III}–NO or Mn^{II}–NO adducts the stretch is higher than the bend (Parthasarathi & Spiro, 1987), reflecting the enhanced back-bonding in the nitrosyl complexes. The present results are the first ones recorded for a Fe^{II}–CN^- adduct, which is also isoelectronic with Fe^{II}–CO. In this case, too, the bend is higher than the stretch, although both frequencies are lower than for Fe^{II}–CO. Back-bonding from Fe^{II} is weaker for CN^- than for CO, as reflected in the higher XY stretching frequency, ~2130 cm^{-1} for CN^- vs ~1950 cm^{-1} for CO (the higher O vs N mass accounts for only 60 cm^{-1} of this difference).

In these adducts, which have a total of six Fe d_π plus ligand π^* electrons, the linear geometry is energetically favored since it maximizes back-bonding (Hoffman et al., 1977). Removal of one electron, as in the CN^- adduct of Fe^{III} heme, maintains the linear geometry but lowers the energy cost for bending, since back-donation is less important. This is reflected in the large decrease in the $FeCN^-$ bending frequency (~80 cm^{-1}) between Fe^{II} (present data) and Fe^{III} [e.g., insect hemoglobin (Yu et al., 1984)], while the FeC stretching frequency remains the same (refer to Table I). The decreased back-bonding might have been expected to lower the FeC frequency in Fe^{III}–CN^-, but this factor is counterbalanced by the increased Coulombic interaction (σ donation) between CN^- and Fe^{III} and Fe^{II}.

When a seventh electron is added to the d_π plus π^* count, as in Fe^{II}–NO adducts, the Fe–X–Y angle is bent to avoid the high cost of putting an electron in a π^* orbital (via rehybridization at the X atom). The Fe–N–O angle is 149° for five-coordinate (NO)Fe^{II}(TPP) but 140° when 1-MeIm is bound axially to this complex (Scheidt & Piciulo, 1976). The angle is steeper, 130°, for O_2 adducts of Fe^{II} heme (Jameson et al., 1978), since the d_π plus π^* electron count is now 8.

Bending of the FeXY equilibrium angle introduces a strong coupling between the FeX stretch and the FeXY bend, since stretching of the FeX bond is assisted by further bending of the FeXY angle. The effect is to mix the two normal modes, which were originally purely stretching and bending, and to drive their frequencies apart (Li & Spiro, 1988). As the angle decreases, the high-frequency mode becomes increasingly stretching in character while the low-frequency mode becomes increasingly bending in character. Despite this progressive change in the mode composition with angle, the high-frequency mode retains its zigzag isotopic pattern, while the low-frequency mode retains its monotonic dependence on the total ligand mass.

The sulfite reductase hemoprotein ligand modes observed in the present study are cataloged in Table I, where they are compared with appropriate heme protein analogues. Structural implications of these data are discussed in the succeeding sections.

NO Adducts. As discussed above, Fe^{II} nitrosyl adducts are intrinsically bent because of their seven d_π plus π^* electron count. The 558-cm^{-1} SiR-HP^{1-}–NO band (548 cm^{-1} at room temperature) corresponds closely to the 554-cm^{-1} band of nitrosyl myoglobin, which also shows a zigzag isotope pattern (Tsubaki & Yu, 1982). Because of this pattern the band was ascribed to FeNO bending, but, on the basis of the kinematic factors (Li & Spiro, 1988) significant Fe–N stretching in character is expected for these bent structures. The expected low-frequency monotonic counterpart band has not been detected for either protein.

The NO stretching frequency is markedly lower for SiR-HP^{1-}, 1555 cm^{-1}, than for Mb, 1624 cm^{-1}. Part of this difference may be due to electronic effects of the different tetrapyrrole macrocycles. Since isobacteriochlorins are easier to oxidize than porphyrins (Change et al., 1981), the Fe atom should be more electron rich, and back-bonding to the NO ligand might be enhanced. This effect has been invoked to account for the higher CO affinity of isobacteriochlorins relative to porphyrins and chlorins (Chang, 1982). It seems

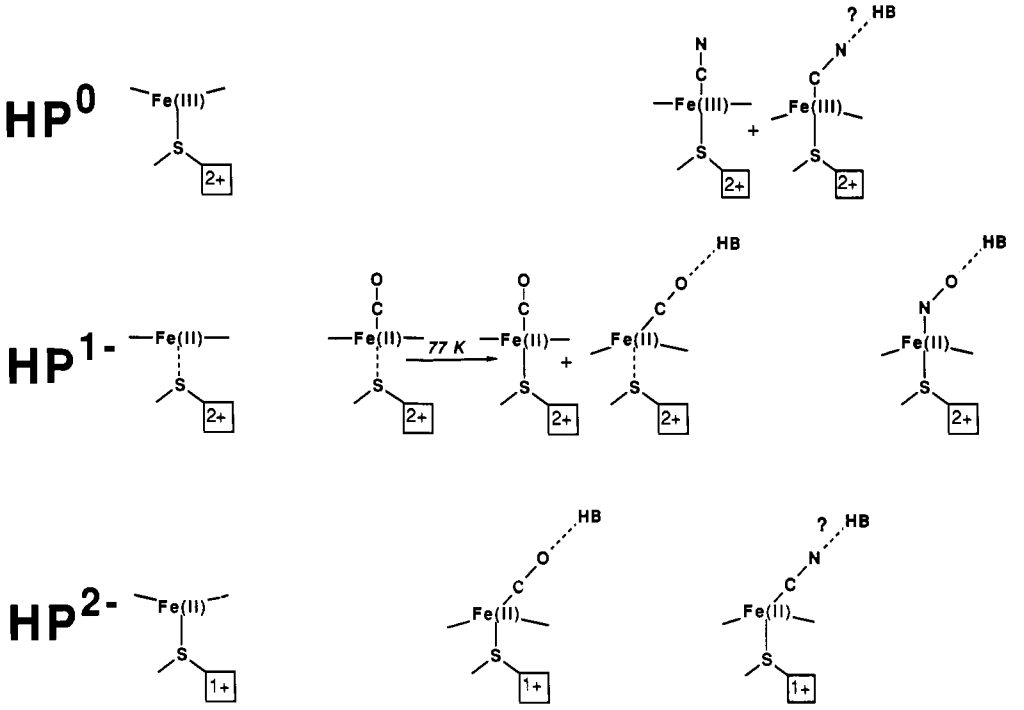

FIGURE 9: Proposed structures of the active site on the basis of the RR data.

unlikely, however, that this effect could produce the 69-cm^{-1} downshift in SiR-HP. More likely there is a distal interaction of the bound NO that increases back-donation; the likeliest interaction would be H-bond donation from a distal side chain. EPR data suggest that the siroheme Fe^{II} in SiR-HP^{1-}–NO is predominantly six-coordinate, yielding a rhombic-type spectrum in the frozen state (Janick et al., 1983). The strong magnetic coupling between the heme and cluster observed in the Mössbauer spectrum (Christner et al., 1983) of SiR-HP^{1-}–NO is in agreement with the hypothesis that a heme Fe^{II}–S bond is present in this species. For these reasons, we tentatively show the siroheme Fe^{II} as six-coordinate in the SiR-HP^{1-}–NO complex in Figure 9, which summarizes our inferences regarding ligand bonding geometries in the various adducts.

CO Adducts. The vibrational data for SiR-HP^{2-}–CO are strikingly similar to those reported for the CO adduct of reduced horseradish peroxidase (Smulevich et al., 1986). The CO stretching frequency is the same, 1904 cm^{-1}, and is 40 cm^{-1} lower than observed in MbCO (Tsubaki et al., 1982). Both proteins show a zigzag mode near 580 cm^{-1} and a monotonic mode near 530 cm^{-1}, although both SiR-HP^{2-}–CO frequencies are 10 cm^{-1} lower than the HRP–CO frequencies. These frequencies are assignable to FeCO bending and FeC stretching, respectively. The small frequency separation between them, 50 cm^{-1}, rules out a significantly bent FeCO structure (Li & Spiro, 1988).

In the case of HRP–CO, distal H-bonding is established as the reason for the anomalously low CO stretching frequency, since the 1904-cm^{-1} infrared band shifts down 2.5 cm^{-1} in D_2O (Smulevich et al., 1986). Likewise, the elevated FeC stretch at 537 cm^{-1}, relative to the ~500-cm^{-1} band seen for protein-free CO–heme–imidazole complexes, is attributable to enhanced back-bonding induced by the distal H-bonding. Similar H-bonding for SiR-HP^{2-}–CO seems possible, especially in view of the anomalously low NO frequency seen in SiR-HP^{1-}–NO. In both HRP–CO and SiR-HP^{2-}–CO the FeCO bending mode is quite strongly activated in the RR spectrum, implying a significant off-axis electronic influence. This is plausibly attributed to the distal H-bond, which may well tilt the FeCO unit significantly relative to the heme plane. Tilting has been shown to be a lower energy distortion coordinate than Fe–CO bending or heme buckling for a given off-axis displacement (Li & Spiro, 1988).

SiR-HP^{1-}–CO displays a significant variation on this structural theme. The CO stretching frequency rises significantly, to 1920 cm^{-1} in solution, and splits into two components at 1910 and 1936 cm^{-1} upon freezing. Correspondingly, there are two Fe–C stretches in frozen solution, at 532 and 504 cm^{-1}. As shown in Table I, we associate the 532-cm^{-1} Fe–C stretch with the 1910-cm^{-1} CO stretch and the 504-cm^{-1} FeC stretch with the 1936-cm^{-1} CO stretch, since back-bonding produces a reciprocal relationship between the FeC and CO stretching frequencies (Yu, 1986; Uno et al., 1987; Li & Spiro, 1988). The 504- and 1936-cm^{-1} peak frequencies are in the range seen for MbCO and other heme CO complexes that lack a specific distal H-bond.

We offer the following interpretation of the spectra. Oxidation of SiR-HP^{2-}–CO to SiR-HP^{1-}–CO involves removal of an electron from the reduced Fe_4S_4 cluster. This should have the effect of decreasing the negative charge on the sulfur atom of the thiolate ligand which is believed to bridge the cluster and the siroheme. As a result, back-bonding from the siroheme Fe to the CO should decrease, thereby strengthening the CO bond. Consistent with such an effect, the CO stretch in SiR-HP^{1-}–CO is seen at 1920 cm^{-1} in the room temperature spectra, significantly higher than the 1904 cm^{-1} observed in room temperature SiR-HP^{2-}–CO. By analogy to HRP, we have suggested that interaction with a distal H-bond donor could contribute to the lowering of the CO stretching frequency in the latter complex. A decrease in back-bonding upon oxidation of the cluster should weaken such an H-bond, if present, by lowering the partial negative charge on the carbonyl oxygen atom. This second effect would also be expected to result in an increase in the CO stretching frequency. The existence of two distinct spectral species in the frozen-state spectra of SiR-HP^{1-} does support the notion of alternative bonding conformations for CO in SiR-HP. The observed 504/1936-cm^{-1} band pair is entirely consistent with a non-H-bonded heme carbonyl, while maintenance of such an H-bond

Table II: Observed and Calculated[a] Frequencies (cm^{-1}) of ν(Fe–CN) and δ(Fe–C–N) for HP^0–CN

	observed				calculated			
mode	ν	$\Delta(^{13}CN)$	$\Delta(C^{15}N)$	$\Delta(^{13}C^{15}N)$	ν	$\Delta(^{13}CN)$	$\Delta(C^{15}N)$	$\Delta(^{13}C^{15}N)$
linear								
ν(Fe–CN)	451	4	4	7	450	5.2	6.2	11.1
δ(Fe–C–N)	390	14	2	16	392	11.2	3.2	14.5
bent								
ν(Fe–CN)	451	17	2	17	453	9.8	3.9	13.9
δ(Fe–C–N)	352	2	4	6	356	6.0	4.7	11.2

[a] Force constants used: linear, K(Fe–C) = 2.20 mdyn/Å, H(Fe–C–N) = 0.41 mdyn·Å/rad^2; bent (Fe–C–N angle of 165°), K = 1.85, H = 0.41. Bond distances used: d(Fe–C) = 1.91 Å, d(C–N) = 1.15 Å.

could account for the 532/1910-cm^{-1} species that, like SiR-HP^{2-}–CO at room temperature, appears similar to the H-bonded form of HRP–CO.

CN^- Adducts. As noted under Results, spectra of the reduced protein cyanide adduct, SiR-HP^{2-}–CN^-, provide the first data on cyanide modes of a heme Fe^{II}–CN^- adduct. This complex is isoelectronic with Fe^{II}–CO, and the spectral pattern is indeed analogous in that a band at 495 cm^{-1} with a zigzag isotope pattern lies above a band at 452 cm^{-1} with a monotonic isotope pattern. Both frequencies are significantly (50–80 cm^{-1}) lower than those seen for CO heme adducts, consistent with weaker back-bonding to CN^- than to CO. A linear $FeCN^-$ unit is implied by the small frequency separation, 43 cm^{-1}, between the two modes, as discussed above. The CN^- stretch has not been detected, and model compound data are not available. Therefore, we are unable to draw inferences about possible distal H-bonding. The substantial RR activation of the $FeCN^-$ bend, however, suggests a significant off-axis perturbation.

Oxidation of the protein again produces a more complex situation. Four isotope-sensitive bands are seen for SiR-HP^0–CN^- (see Figure 8), two with zigzag and two with monotonic isotope patterns. Two different structures are implied, just as in the case of SiR-HP^{1-}–CO; previous EPR data have already suggested the possibility of multiple species in SiR-HP^0–CN^- in frozen solutions (Janick, 1983). There are two ways to pair the bands: (a) 451 cm^{-1} (monotonic) with 390 cm^{-1} (zigzag) and 352 cm^{-1} (monotonic) with 451 cm^{-1} (zigzag); or (b) 451 cm^{-1} (monotonic) with 451 cm^{-1} (zigzag) and 352 cm^{-1} (monotonic) with 390 cm^{-1} (zigzag). Neither combination can be ruled out a priori, but combination b implies large differences in both Fe–C stretching and Fe–C–N bending force constants between the two adducts, for which it is hard to find a physical rationale. Combination a, on the other hand, has a reasonable explanation if the second pair belongs to a bent complex. As noted above, for linear FeXY adducts the stretch and bend are uncoupled and either one may lie higher. But when FeXY is bent a large coupling is introduced, which mixes the modes and drives them apart; the higher frequency mode retains the zigzag isotope pattern. This coupling can explain the large frequency separation of the 352/451-cm^{-1} band pair if the FeCN angle is significantly bent, while the 451/390-cm^{-1} band pair is consistent with a linear structure, and the frequencies are similar to those shown by the Fe^{III}–CN^- adduct of an insect hemoglobin [451 cm^{-1} (monotonic) and 412 cm^{-1} (zigzag) (Benko & Yu, 1983; Gersonde et al., 1987)]. As shown in Table II, we are able to calculate the frequencies of both band pairs with a simple triatomic model using linear and 165° bent $FeCN^-$. The bending force constant is the same in both cases, but the Fe–C stretching constant has to be decreased by ~20% for the bent structure. The isotope shifts are well reproduced for the linear structure, but deviate somewhat from the observed values for the bent structure, although the basic trend is maintained. Part of this discrepancy may be experimental, due to the band overlaps in the spectra, but part is no doubt due to the oversimplification of the model. In particular, the lowered FeC stretching constant implies a significant electronic perturbation of the bent structure. This may be attributable to distal H-bonding, which would be expected to lower the effective charge on the CN^- ligand and therefore its σ-donating tendency, which is probably the main determinant of the Fe–CN^- bond strength. Such an H-bond would produce kinematic as well as electronic effects and would no doubt alter the isotope shift pattern.

The calculation adds plausibility to the interpretation of the data in terms of a mixture of linear and bent structures. As far as we can tell, this is the first vibrational spectroscopic evidence for bending of a normally linearly coordinated heme ligand. Although Fe–CO bending has been advanced to explain the off-axis bonding of CO in myoglobin and other heme proteins, significant FeCO bending is inconsistent with available vibrational data (Kerr et al., 1983), as discussed above. Tilting rather than bending is the preferred distortion mode for FeCO, due to the higher energy cost of bending, which is associated with the loss of back-bonding (Hoffman et al., 1977). It is reasonable, however, that bending could occur for CN^- adducts of Fe^{III}, for which back-bonding is much less important and for which the bending frequency, and therefore the bending force constant, is much lower than in Fe–CO adducts. Such bonding might be facilitated by interaction of the bent CN^- ligand with a distal H-bonding group.

Conclusions. The RR spectra presented here provide vibrational data on a number of ligand complexes of SiR-HP at three distinct reduction levels. A possible interpretation of the data is presented schematically in Figure 9. Comparison of the ligand vibrational frequencies observed in SiR-HP with those of other heme proteins and models demonstrates the presence of steric and/or electronic interactions capable of significantly lowering the X–Y vibrational frequency of the diatomic ligands CO and NO and of altering the mixing between the stretching and bending modes of the Fe–X–Y triatomic unit. The existence of more than one distinct spectral form in two of the enzyme adducts investigated here suggests the presence of alternative bonding geometries.

In principle, heme ligand vibrational frequencies can be affected either by distal interactions, such as H-bonding to the bound ligand, steric hindrance, or electronic interactions with nearby side chains, or by proximal interactions involving alterations in the backside heme electronic environment. For SiR-HP, a consideration of the functional requirements of the catalytic cycle leads to the expectation that both types of interactions might be encountered. Since the six-electron reduction of substrate, SO_3^{2-}, is necessarily accompanied by three dehydrations, there is an obvious role for one or more proton donors in the ligand binding pocket. Equally important, bond angle distortion induced by siroheme pocket H-bond

donors could be significant in regulating the electron affinity of the bound nitrogen oxide (Enemark & Feltham, 1972) or sulfur oxide (Ryan & Eller, 1976) ligand during the initial phases of the six-electron reduction catalyzed by SiR-HP. We have pointed out the similarity of certain of the CO-bound spectral forms of SiR-HP to those seen in the H-bonded complex of HRP and have suggested that interactions with an H-bond donor could also account for the spectral heterogeneity of the oxidized cyanide adduct and the inferred geometric distortion in these species. Direct RR evidence for such an H-bond will require further studies. At the same time, the presence of the redox-active Fe_4S_4 cluster, which we here assume provides the siroheme backside sulfur ligand as proposed in the bridging model of the SiR-HP active site, provides a mechanism for modulating the electron-donor properties of the siroheme iron. The two types of effect may have dynamic interactions, as proposed in the discussion of the CO species, since an enhancement in the electron-donor properties of the siroheme iron secondary to cluster reduction could strengthen a distal H-bond. Conversely, cluster oxidation or weakening of the heme cluster bridging bond could have the opposite effect, facilitating breakage of a distal H-bond.

Registry No. Fe, 7439-89-6; ^{13}C, 14762-74-4; O_2, 7782-44-7; $^{18}O_2$, 14797-71-8; N_2, 7727-37-9.

References

Baldwin, J. M. (1980) *J. Mol. Biol. 136*, 103–128.

Benko, B., & Yu, N.-T. (1983) *Proc. Natl. Acad. Sci. U.S.A. 80*, 7042–7046.

Chang, C. K. (1982) in *The Biological Chemistry of Iron* (Dunford, H. B., Dolphin, D., Raymond, K. N., & Sieker, L., Eds.) pp 313–334, Reidel, Dordrecht, The Netherlands.

Chang, C. K., Hanson, L. K., Richardson, P. F., Young, R., & Fajer, J. (1981) *Proc. Natl. Acad. Sci. U.S.A. 78*, 2652–2656.

Christner, J. A., Janick, P. A., Siegel, L. M., & Münck, E. (1983) *J. Biol. Chem. 258*, 11157–11164.

Czernuszewicz, R. S., & Johnson, M. K. (1983) *Appl. Spectrosc. 37*, 297–298.

Enemark, J. H., & Feltham, R. D. (1972) *Proc. Natl. Acad. Sci. U.S.A. 69*, 3534–3536.

Gersonde, K., Yu., N.-T., Kerr, E. A., Smith, K. M., & Parish, D. W. (1987) *J. Mol. Biol. 194*, 545–556.

Han, S., Madden, J. F., Thompson, R. G., Strauss, S. H., Siegel, L. M., & Spiro, T. G. (1989) *Biochemistry* (first of three papers in this issue).

Heidner, E. J., Ladner, R. C., & Perutz, M. F. (1976) *J. Mol. Biol. 104*, 707–722.

Hoffman, R., Chen, M. L., & Thorn, D. L. (1977) *Inorg. Chem. 16*, 504–505.

Jameson, G. B., Rodley, G. A., Robinson, W. T., Gagne, R. R., Reed, C. A., & Collman, J. P. (1978) *Inorg. Chem. 17*, 850–857.

Janick, P. A. (1982) Ph.D. Thesis, Duke University.

Janick, P. A., & Siegel, L. M. (1983) *Biochemistry 22*, 504–515.

Janick, P. A., Rueger, D. C., Krueger, R. J., Barber, M. J., & Siegel, L. M. (1983) *Biochemistry 22*, 396–408.

Kerr, E. A., & Yu, N.-T. (1988) in *Biological Applications of Raman Spectroscopy* (Spiro, T. G., Ed.) Vol. 3, pp 39–95, Wiley-Interscience, New York.

Kerr, E. A., Mackin, H. C., & Yu, N.-T. (1983) *Biochemistry 22*, 4373–4379.

Kuriyan, J., Wilz, S., Karplus, M., & Petsko, G. A. (1986) *J. Mol. Biol. 192*, 133–154.

Li, X.-Y., & Spiro, T. G. (1988) *J. Am. Chem. Soc. 110*, 6024–6033.

Madden, J. F., Han, S., Siegel, L. M., & Spiro, T. G. (1989) *Biochemistry* (second of three papers in this issue).

Maxwell, J. C., & Caughey, W. S. (1976) *Biochemistry 15*, 388–396.

McRee, D. E., Richardson, D. C., Richardson, J. S., & Siegel, L. M. (1986) *J. Biol. Chem. 261*, 10277–10281.

Murphy, M. J., Siegel, L. M., & Kamin, H. (1974) *J. Biol. Chem. 249*, 1610–1614.

Ogino, H., Shimura, M., & Tanaka, N. (1979) *Inorg. Chem. 18*, 2497–2501.

Parthasarathi, N., & Spiro, T. G. (1987) *Inorg. Chem. 26*, 2280–2282.

Rueger, D. C., & Siegel, L. M. (1976) in *Flavins and Flavoproteins* (Singer, T. P., Ed.) pp 610–620, Elsevier, New York.

Ryan, R. R., & Eller, P. G. (1976) *Inorg. Chem. 15*, 494–496.

Scheidt, W. R., & Piciulo, P. L. (1976) *J. Am. Chem. Soc. 98*, 1913–1919.

Siegel, L. M., & Davis, P. S. (1974) *J. Biol. Chem. 249*, 1587–1598.

Smulevich, G., Evangelista-Kirkup, R., English, A., & Spiro, T. G. (1986) *Biochemistry 25*, 4426–4430.

Steigmann, W., & Weber, E. (1979) *J. Mol. Biol. 127*, 309–338.

Tsubaki, M., & Yu, N.-T. (1982) *Biochemistry 21*, 1140–1144.

Tsubaki, M., Srivastava, R. B., & Yu, N.-T. (1982) *Biochemistry 21*, 1132–1140.

Uno, T., Nishimura, Y., Tsuboi, M., Makino, R., Iizuka, T., & Ishimura, Y. (1987) *J. Biol. Chem. 262*, 4549–4556.

Van Etten, R. L., & Risley, J. M. (1981) *J. Am. Chem. Soc. 103*, 5633–5636.

Yoshikawa, S., O'Keefe, D. H., & Caughey, W. S. (1985) *J. Biol. Chem. 260*, 3518–3528.

Yu, N.-T. (1986) *Methods Enzymol. 130*, 350–409.

Yu, N.-T., Kerr, E. A., Ward, B., & Chang, C. K. (1983) *Biochemistry 22*, 4534–4540.

Yu, N.-T., Benko, B., Kerr, E. A., & Gersonde, K. (1984) *Proc. Natl. Acad. Sci. U.S.A. 81*, 5106–5110.